



**HAL**  
open science

## Added value of MRI for the diagnosis of adnexal torsion in children and adolescents after inconclusive ultrasound examination

E. Rougier, W. Mar, V. Della Valle, B. Morel, S. Irtan, E. Audureau, A. Coulomb-L'hermine, H. Ducou Le Pointe, E. Blondiaux

### ► To cite this version:

E. Rougier, W. Mar, V. Della Valle, B. Morel, S. Irtan, et al.. Added value of MRI for the diagnosis of adnexal torsion in children and adolescents after inconclusive ultrasound examination. *Diagnostic and Interventional Imaging*, 2020, 101, pp.747 - 756. 10.1016/j.diii.2020.04.015 . hal-03493438

**HAL Id: hal-03493438**

**<https://hal.science/hal-03493438>**

Submitted on 7 Nov 2022

**HAL** is a multi-disciplinary open access archive for the deposit and dissemination of scientific research documents, whether they are published or not. The documents may come from teaching and research institutions in France or abroad, or from public or private research centers.

L'archive ouverte pluridisciplinaire **HAL**, est destinée au dépôt et à la diffusion de documents scientifiques de niveau recherche, publiés ou non, émanant des établissements d'enseignement et de recherche français ou étrangers, des laboratoires publics ou privés.



Distributed under a Creative Commons Attribution - NonCommercial 4.0 International License

# Added value of MRI for the diagnosis of adnexal torsion in children and adolescents after inconclusive ultrasound examination

Short title:

## MRI in pediatric adnexal torsion

Elodie ROUGIER <sup>a</sup>, Winnie MAR <sup>b</sup>, Valeria DELLA VALLE <sup>a</sup>, Baptiste MOREL <sup>a</sup>,  
Sabine IRTAN <sup>c</sup>, Etienne AUDUREAU <sup>d</sup>, Aurore COULOMB-L'HERMINE <sup>e</sup>, Hubert  
DUCOU LE POINTE <sup>a</sup>, Eléonore BLONDIAUX <sup>a\*</sup>

### Affiliations

<sup>a</sup>. Department of Imaging; Hôpital Trousseau – Hôpitaux Universitaires de l'Est Parisien,  
Assistance Publique - Hôpitaux de Paris, Sorbonne Université, 75012, Paris, France

<sup>b</sup>Department of Radiology University of Illinois at Chicago, Chicago, IL 60612, USE

<sup>c</sup>Department of Surgery ; Hôpital Trousseau – Hôpitaux Universitaires de l'Est Parisien,  
Assistance Publique - Hôpitaux de Paris, Sorbonne Université, 75012 Paris, France

<sup>d</sup>Biostatistic and Epidemiology Department; Hôpital Henri Mondor, Assistance Publique -  
Hôpitaux de Paris, LIC EA 4393, Université Paris-Est Créteil, 91000 Créteil, France

<sup>e</sup>Department of Pathology; Hôpital Trousseau – Hôpitaux Universitaires de l'Est Parisien,  
Assistance Publique - Hôpitaux de Paris, Sorbonne Université, 75012 Paris, France

\*Corresponding author: [eleonore.blondiaux@aphp.fr](mailto:eleonore.blondiaux@aphp.fr)

Sorbonne Université, Assistance Publique - Hôpitaux de Paris, Department of Radiology,  
Hôpital Armand-Trousseau, 26 Avenue du Dr Arnold Netter, 75012 Paris, France. Telephone:  
+33 1 44 73 62 10

## Abstract

**Purpose.** The purpose of this study was to assess the performance of magnetic resonance imaging (MRI) in children and adolescents with suspected adnexal torsion (AT) after inconclusive initial ultrasound examination.

**Materials and methods.** Twenty-eight girls with a mean age of  $12 \pm 4$  (SD) years (range: 1 month to 18 years) were included. All had clinically suspected AT and inconclusive initial ultrasound findings followed by pelvic MRI as a second-line imaging modality. The final diagnosis was obtained by surgery or follow-up. Two radiologists blinded to the clinical, ultrasound and surgical data, retrospectively and independently reviewed MRI examinations. Clinical and MRI features associated with AT were searched for using univariate analyses.

**Result.** Among the 28 patients, 10/28 patients (36%) had AT and 22/28 (79%) had an ovarian or tubal mass. AT was associated with an age  $< 13$  years (OR: 10.7; 95% CI: 1.3 - 148.2) ( $P = 0.022$ ) and a whirlpool sign at MRI (OR: 61.0; median unbiased estimate, 7.2) ( $P < 0.0001$ ). When a mass was present, the best quantitative MRI criteria for AT were mass volume and ovary-corrected volume  $\geq 30 \text{ cm}^3$  ( $\kappa = 0.72$  and  $0.61$ , respectively), mass axis length  $\geq 5 \text{ cm}$  ( $\kappa = 0.90$ ), and mass surface area  $\geq 14 \text{ cm}^2$  ( $\kappa = 0.58$ ), with moderate to almost perfect interobserver agreement. The overall sensitivity, specificity and accuracy of MRI for the diagnosis of AT were 100% (10/10; 95% CI: 69 -100), 94% (17/18; 95% CI: 73 - 100) and 96% (27/28; 95% CI: 82 - 100) respectively, with perfect interobserver agreement ( $\kappa = 1$ ).

**Conclusion.** In pediatric patients with suspected AT and inconclusive initial ultrasound examination, a strategy including MRI as a second-line imaging modality should be considered if MRI does not delay a potential surgery.

**Keywords:** Adnexal torsion; Ovarian torsion; Child; Ultrasonography; Magnetic resonance imaging (MRI)

## Abbreviations

AT: Adnexal torsion

AUC: area under the receiver operating curve

MRI: Magnetic resonance imaging

OR: odds ratio

ROC: receiver operating curve

SD: standard deviation

## **Introduction**

Adnexal torsion (AT) is a rare condition in the pediatric population with an estimated incidence of 4.9/100000 females aged from 1 year to 20 years [1]. Early diagnosis of AT is essential because delayed identification may lead to ovarian hemorrhagic infarction and necrosis of adnexal structures, which may impair future fertility [2]. Generally, ultrasound is the initial investigation when clinical findings are consistent with AT [3]. In adults, ultrasound may demonstrate key signs of AT such as an enlarged ovary, abnormal flow on color Doppler ultrasound, peripherally displaced follicles, an adnexal mass that may trigger AT, a thickened ovarian tube and a whirlpool sign [4, 5]. Ultrasound findings in children with AT have also been described [6, 7], with overall high sensitivity (90.9%) but relatively low specificity (68.7%) and accuracy (80%) [8]. In few children, ultrasound examination cannot exclude torsion with certainty mostly because ultrasound findings in AT overlap with those of simple hemorrhagic cyst that may mimic AT. Moreover, in children with a large ovarian mass stretching the ovarian parenchyma, the usual ovarian signs of AT are missing. Therefore, with an inconclusive initial ultrasound examination, additional strategies are needed to improve the diagnostic accuracy and decrease the rate of diagnostic laparoscopy, because the latter can be associated with substantial morbidity.

In studies of adults with suspected AT, magnetic resonance imaging (MRI) has shown high accuracy in the diagnosis of AT [9, 10]. Moreover, pelvic MRI may provide information regarding the actual nature of a pelvic mass [11]. In children, beyond the advantage of lack of ionizing radiation and excellent soft-tissue contrast provided by MRI, the diagnostic accuracy of MRI for suspected AT in children has not been reported.

The purpose of this study was to retrospectively assess the value of MRI for the diagnosis of AT in children and adolescents after inconclusive initial ultrasound examination.

## **Materials and methods**

### *Population*

We reviewed patients with suspected AT with an inconclusive ultrasound examination as a first-line imaging modality that required MRI as a second-line technique between 2010 and 2017.

Patients were further included when the final diagnosis was confirmed after surgery and/or clinical and imaging follow-up for at least 3 months. Patients with other diagnosis than AT were excluded as well as those who did not undergo ultrasound follow-up after the initial ultrasound. Figure 1 shows patients inclusion/exclusion process into the study. All procedures were in accordance with the ethical standards of the local ethics committee on human experimentation. Informed consent was not required due to the retrospective design of the study.

A total of 28 girls with a mean age of  $12 \pm 4$  (standard deviation [SD]) years (range: 1 month - 18 years) were evaluated for suspected AT with an initial inconclusive ultrasound examination followed by pelvic MRI. Demographic and clinical data of included patients were recorded.

### *Ultrasound examination*

*Initial ultrasound examination.* Ultrasound was performed with Aplio<sup>®</sup> 400 or 500 ultrasound devices (Toshiba Medical Systems Corporation) with a 5- to 8-MHz curved array and 7- to 12-MHz linear probes and included complete examination of the abdomen and pelvis. Endovaginal ultrasound was not performed in this pediatric population. Ultrasound was performed by pediatric radiologists with at least 6 years of experience with abdominal ultrasound or by residents under supervision by a certified pediatric radiologist.

*Ultrasound follow-up.* Patients who had no MRI findings consistent with AT and no surgery, underwent ultrasound follow-up. A second ultrasound examination was performed within the first week after the initial ultrasound, followed by a third ultrasound examination between 6 and 8 weeks after the initial ultrasound. Pain reduction associated with an ultrasound appearance of a collapsed hemorrhagic cyst confirmed the absence of AT. Moreover, when surgery was performed, the presence of an involution or a normal appearance of the ovary was recorded at ultrasound follow-up.

### *MRI examination*

#### **MRI protocol**

MRI examination was performed with a 1.5-Tesla system (Achieva<sup>®</sup>, Philips Medical Systems) with a phased-array pelvic coil for optimal signal-to-noise ratio. One patient underwent MRI examination under sedation and one with postprandial swaddling. MRI examinations were performed using various protocols, including at least the following sequences: sagittal and axial

turbo spin echo T2-weighted sequences and axial gradient-echo T1-weighted sequences with and without fat signal suppression. Delayed contrast-enhanced axial and sagittal gradient-echo T1-weighted sequences after intravenous administration of a gadolinium chelate (Gadoterate meglumine, Dotarem<sup>®</sup>, Guerbet) were obtained for 21 patients (1 minute after intravenous injection of 0.02 mL/kg) Three patients underwent pelvic MR diffusion imaging. All MRI examinations were performed within a few hours after initial ultrasound examination.

### **MR image analysis**

MR images were reviewed retrospectively on a picture-archiving workstation by two independent radiologists (E.B. and E.R.) with 15- and 4-years of experience in pediatric MRI, respectively, who were blinded to the surgical and pathological data. Each reader worked independently blinded to the results of the original interpretation and to the final diagnosis. Readers were asked to provide the most plausible diagnosis. No patients were excluded due to poor MRI examination quality. MR images were analyzed qualitatively and quantitatively.

*Qualitative data.* MR images of the ovary were evaluated for presence of ovarian stromal edema, peripheral distribution of follicles, asymmetric ovarian parenchymal enhancement and ovarian shift to the involved side. Regarding the adnexa, the following features were noted: thickening or dilatation of the fallopian tube (comparatively with controlateral tube), presence of a whirlpool sign (twisted ovarian pedicle or fallopian tube), defect of enhancement of tubal wall on the pathological side, vascular pedicle enlargement (comparatively with controlateral), inflammatory pelvic fat, and uterine displacement. Moreover, the presence of an adnexal mass and its characteristics were noted: solid and/or cystic components with or without fat stranding or hemorrhagic content (*e.g.*, hyperintensity on T1-weighted and T2-weighted images or presence of a fluid-fluid level in cyst with hemorrhagic content). Etiological hypotheses regarding the mass on MR images included functional follicular and paratubal cysts with or without hemorrhage and ovarian teratoma.

*Quantitative data.* For each ovary, the following variables were retrospectively measured: ovary alone (ovary-corrected surface and volume), mass alone (axis/diameter, surface, volume), and ovary and mass together (total axis/diameter, total surface, total volume). For this, each radiologist performed measurements on axial MR images for ovarian dimensions and ovarian, axial and sagittal sections for ovarian volume measurements. The choice of sections was at the discretion of the radiologist who selected the images on which the ovarian dimensions were the largest. The ratios of the dimensions of the abnormal to the normal contralateral ovary were

calculated.

After independent reading of which results were used to calculate interobserver agreement, discordant opinions were resolved by a consensus reading. The results of the consensus reading were used for further statistical analysis.

### **Standard of reference**

Among the 28 patients, 10/28 (36%) had AT and 18/28 (64%) had no AT. In the 10 patients with AT, the diagnosis was confirmed by surgery as a standard of reference as follows: intraoperative findings of an enlarged ovary associated with a torsion of the adnexal tube. The ovary was non-viable in 8 and oophorectomy was performed. Ovarian necrosis was confirmed by pathology in these 8 patients. Conservative treatment with detorsion was performed in 2 patients with AT. In the 18 patients without AT, the diagnosis was assessed using laparoscopy or follow-up. In 6 patients, laparoscopy was performed after MRI and found a luteal hemorrhagic cyst with an ovary and adnexa of normal aspect. In 12 patients, clinical and ultrasound follow-up confirmed the diagnosis of hemorrhagic cyst with typical signs of clot involution and visualization of a normal echo structure and size of the ovarian parenchyma.

A total of 22/28 (79%) patients had an ovarian or a tubal mass: for 17/28 (61%), these were cysts with hemorrhagic content (16 ovarian functional cysts and 1 paratubal cyst) and for 4/28 (14%), they were ovarian teratomas. One patient had a paratubal cyst without hemorrhagic content.

### **Statistical analysis**

Quantitative variables were expressed as means  $\pm$  standard deviation [SD], and ranges. Qualitative data were expressed as raw numbers, proportions and percentages.

The diagnostic performance analysis of MRI was conducted based on the consensus results by considering the final diagnosis of AT. To identify factors associated with the diagnosis of AT on MRI, we compared patients with AT and those without AT. Categorical (qualitative) variables were compared using the chi-square or Fisher's exact tests. Continuous (quantitative) variables were compared using the Student *t* test or Mann–Whitney test after normality of the distribution has been checked using the Shapiro-Wilk test. The relationships between each MRI criteria and the diagnosis of AT was tested by univariate or exact univariate logistic regression analysis. The exact method was used when there was a complete separation of data.

Quantitative variables on MRI were dichotomized after optimal thresholds were determined by identifying the value with the maximal Youden's index and the shortest distance from the upper-left corner on receiver operating curve (ROC) analysis. Corresponding odds ratios (OR) along with their 95% confidence intervals (95% CI) and area under the ROC curve (AUC) were computed by unadjusted exact logistic regression to account for the relatively low sample size of the study and the occurrence of null percentages cells. Significance was set at  $P < 0.05$ .

For each categorical variable on MRI, sensitivity, specificity were estimated and the 95% exact CI were calculated.

The Kappa coefficients were computed along with their 95% CI to assess inter observer agreement (senior vs. junior radiologist) in terms of MRI findings. Degrees of agreement were categorized as follows: 0.00–0.20, slight agreement; 0.21–0.40, fair agreement; 0.41–0.60, moderate agreement; 0.61–0.80, substantial agreement; and 0.81–1.00, almost perfect agreement [12]. In addition, the proportion of agreement was calculated for all qualitative variables.

All statistical analyses were performed using Stata software version v15.1 (StataCorp LP, College Station, Texas, USA).

## Results

Mean age was lower in patients with AT ( $9 \pm 5$  [SD] years; range: 4 months- 15 years) than in those without AT ( $14 \pm 1$  [SD] years; range: 11-16 years) ( $P = 0.01$ ). Table 1 shows the distribution of MRI findings in patients with AT and those without AT. The whirlpool sign ( $P < 0.001$ ), tubal thickening ( $P = 0.0001$ ), presence of ovarian T1-weighted hyperintensity ( $P = 0.032$ ) (Figure 2) and vascular pedicle enlargement ( $P = 0.041$ ) were more frequently observed in patients with AT than in those without AT (Table 1). AT was more frequent with a mature cystic teratoma versus no mass ( $P = 0.003$ ). Among patients with hemorrhagic cysts, AT was found in 2/17 patients (12%) (Figure 3). The remaining categorical variables were not associated with AT (Figures 4 and 5).

The results of quantitative analysis are presented in Table 2. When a mass was present on MRI, patients with AT had a larger mass, larger adnexal mass surface and larger adnexal mass volume than those without AT (Table 2).

Table 3 shows the results of univariate analysis with exact logistic regression to determine the most discriminative MRI variable to differentiate between patients with AT and those without AT. An age  $< 13$  years was associated with AT (OR: 10.7; 95% CI: 1.3 - 148.2) ( $P = 0.022$ ).

Regarding MRI features, univariate logistic regression analysis showed significant positive association between presence of a whirlpool sign and AT (OR: 61.0; median unbiased estimate, 7.2) ( $P < 0.0001$ ). Tube thickening, absence of a cystic mass with hemorrhagic content, vascular pedicle enlargement and asymmetric ovarian enhancement were also associated with AT. In patients with adnexal mass, qualitative MRI features associated with AT were mass volume and abnormal ovary-corrected volume  $\geq 30 \text{ cm}^3$ , axis length  $\geq 5 \text{ cm}$ , and surface area  $\geq 14 \text{ cm}^2$  (Table 3).

The sensitivity, specificity and accuracy of each MRI variables for the diagnosis of AT are reported in Table 4. The single patient falsely positive for AT had a hemorrhagic cyst seen at laparoscopy. The overall accuracy of MRI for the diagnosis of AT was 96% (27/28; 95% CI: 82 - 100%) and sensitivity 100% (10/10; 95% CI: 69 - 100), specificity 94% (17/18; 95% CI: 73 - 100), with perfect interobserver agreement ( $\kappa = 1$  [95%CI: 1.00 - 1.00]) (Table 5). The most accurate variables for the diagnosis of AT were the presence of a whirlpool sign and a corrected volume of the abnormal ovary  $\geq 30 \text{ cm}^3$ , with substantial interobserver agreement ( $\kappa = 0.62$  [95% CI: 0.29 - 0.95] and  $\kappa = 0.61$  [95% CI: 0.14 - 1.00], respectively).

## Discussion

The results of our study reveal that MRI had high degrees of accuracy, sensitivity and specificity for the diagnosis of AT in children after an inconclusive initial ultrasound examination. Also, agreement between two readers with 4 to 15 years of experience in MRI was perfect. Therefore, a strategy of ultrasound as the first step followed by MRI in patients with inconclusive ultrasound examination for the diagnosis of AT appears to be helpful.

Ultrasound is usually used for first-line imaging work-up in children with suspected AT in the emergency department. However, previous studies of the diagnosis of AT in children reported an overall sensitivity of ultrasound ranging from 51% [13] to 90.9% and low specificity (68.7%) [8]. Ultrasound evaluation of ovaries might be more challenging in children than adults. The ovaries in neonates can be small and may not be found in the pelvis but in a more cranial position [14] or in a herniated canal of Nuck [15]. Moreover, detailed evaluation of the ovaries has been described in adults by using a transvaginal approach that should not be performed in children and rarely in adolescents. Due to these limitations two main sources of inconclusive ultrasound examination in children and adolescents have been identified: hemorrhagic cysts and the presence of a large mass that stretches the ovarian parenchyma and precludes its precise evaluation [8].

Consequently, to assess ovarian torsion in children, other methods should be used in cases of inconclusive initial ultrasound examination [1]. Oltmann et al. reported that a strategy of diagnostic laparoscopy used as a first-line examination in children, particularly those with a pelvic mass  $\geq 5$  cm, may improve ovarian salvage as compared with ultrasound [13]. However, such a strategy may lead to a high rate of surgery in false-positive cases because clinical and laboratory findings are non-specific in AT. Moreover, surgery may cause adhesions in the pelvic cavity that may predispose to AT [16]. As reported by Chiou et al. in a series of AT in adults, 48% of patients had a history of abdominal/pelvis surgery [16].

CT may represent a second-line imaging modality for the diagnosis of AT because it is widely available in emergency settings. In a recent survey, CT has even been reported as a first-line examination modality for the diagnosis of AT in children or adolescents referred for pelvic pain in adult hospitals as compared with pediatric hospitals, where ultrasound is preferred [17]. Although AT findings have been described by CT in children in a few pictorial reviews [2, 4] and in a study of 3 pre-menarchal girls [18], the use of CT to primarily diagnose ovarian torsion is not supported by the literature. In adults and children, Chiou et al. demonstrated that although CT shows features suggestive of torsion, the diagnostic value of initial CT is less than that of initial ultrasound [16]. In adults, Swenson et al. reported that the diagnostic performance of CT does not significantly differ from that of ultrasound in identifying ovarian torsion [19]. Moreover, unlike ultrasound and MRI, CT exposes children to ionizing radiation and has lower contrast resolution as compared with MRI.

To date, the radiology literature describing MRI features for the diagnosis of AT in children consists mainly of single case reports [20-22]. Two retrospective studies including a small number of children demonstrated the ability of MRI to detect AT: 6/58 patients aged 12 to 17 years in the study by Chiou et al. and 25 patients aged between 5- and 85 years (median 40 years) in the study by Rha et al. [16, 23]. However, neither was exclusive to the pediatric population.

In our series, the two main criteria associated with AT were an age under 13 years and a whirlpool sign. In pre-menarcheal girls, AT occurs more often without an ovarian or tubal mass [8]. Similarly, a predictor of AT in our study and premenarchal girl was the absence of a cystic mass with hemorrhagic content. In our study, hemorrhagic functional cysts are exclusively seen in menarcheal girls and corresponded to the main differential diagnosis of AT. Moreover, presence of AT was associated with a large mass, with volume  $\geq 30$  cm<sup>3</sup>, axis length  $\geq 5$  cm and surface area  $\geq 14$  cm<sup>2</sup>. In our series, these large masses were represented essentially by mature

cystic teratomas, as in other studies [2, 7].

The presence of a whirlpool sign on MRI had the strongest association with AT, with substantial inter-reader agreement. In a recent study evaluating the value of MRI for the diagnosis of AT in adults with an equivocal adnexal mass seen on ultrasound, Beranger-Gilbert et al. found a whirlpool sign and thickened tube as MRI features associated with AT [9]. Although the whirlpool sign, a direct representation of the twisted pedicle and tube, has been described on ultrasound in adults [24], it is hardly identified in children on ultrasound [8]. Therefore, MRI, showing more easily this sign, can be used as an accurate second-line imaging modality. Other MRI features associated with a diagnosis of AT on univariate analysis were tube thickening, vascular pedicle enlargement and asymmetric ovarian enhancement. For the last two features, the inter-reader agreement was poor to fair, which may indicate that identification of these two signs depends on the experience of the MRI reader and should prompt specific training among radiology residents.

The rate of oophorectomy was relatively high in our study as compared with most recent studies, with 50% oophorectomy performed for ovarian necrosis [25, 26]. This result may account for the delay between the onset of symptoms and the initial ultrasound in this group of children and the delay between the initial ultrasound and pelvic MRI, although MRI was performed within a few hours after the initial ultrasound in our centre which has good availability of MRI. Recent recommendations specified that MRI should not be performed if it delays the potential surgery [1]. Although the availability of MRI has increased in most pediatric centers in emergency settings, the need for sedation to avoid motion artifacts in young patients and the long examination time with MRI may lengthen a diagnostic algorithm including MRI as a second-line imaging modality.

Our study has some limitations. First, MR images were read by experienced pediatric radiologists. Therefore, our results cannot be generalized to most radiologists in daily practice who do not have similar experience. Second, we did not include patients with acute pelvic pain and negative ultrasound examination because we assumed that the ultrasound examination had ruled out AT. Therefore, the number of patients with false-negative findings might have been underestimated. Third, although this is the first exclusive pediatric study to specifically evaluate MRI features for the diagnosis of AT, the number of patients with AT was limited. Fourth, we did not compare ultrasound and MRI features associated with AT. Because the radiologists ended their initial ultrasound reports with “cannot rule out adnexal torsion”, we considered that we could not retrospectively review ultrasound images and perform a head-to-head comparison

of ultrasound and MRI data. Finally, in a context in which gadolinium-based contrast agents should be used judiciously in children, techniques such as diffusion MRI could represent an alternative to sequences with contrast media administration [27-30]. Only three children underwent pelvic diffusion sequences in our series. Therefore, we could not compare the two techniques.

In conclusion, in children with suspected AT and an inconclusive initial ultrasound examination, MRI as a second-line imaging modality has high sensitivity and accuracy for the diagnosis of AT. We found that tubal thickening and whirlpool signs are potential MRI signs to improve sensitivity in patients with equivocal ultrasound findings. However, such a strategy should not delay potential surgery.

## **Conflict of interest**

The authors report no conflict of interest

## References

- [1] Riccabona M, Lobo ML, Ording-Muller LS, Thomas Augdal A, Fred Avni E, Blickman J, et al. European Society of Paediatric Radiology abdominal imaging task force recommendations in paediatric uroradiology, part IX: Imaging in anorectal and cloacal malformation, imaging in childhood ovarian torsion, and efforts in standardising paediatric uroradiology terminology. *Pediatr Radiol* 2017;4710:1369-80.
- [2] Ngo AV, Otjen JP, Parisi MT, Ferguson MR, Otto RK, Stanescu AL. Pediatric ovarian torsion: a pictorial review. *Pediatr Radiol* 2015;4512:1845-55.
- [3] Bronstein ME, Pandya S, Snyder CW, Shi Q, Muensterer OJ. A meta-analysis of B-mode ultrasound, Doppler ultrasound, and computed tomography to diagnose pediatric ovarian torsion. *Eur J Pediatr Surg* 2015;251:82-6.
- [4] Chang HC, Bhatt S, Dogra VS. Pearls and pitfalls in diagnosis of ovarian torsion. *Radiographics* 2008;285:1355-68.
- [5] Mashiach R, Melamed N, Gilad N, Ben-Shitrit G, Meizner I. Sonographic diagnosis of ovarian torsion: accuracy and predictive factors. *J Ultrasound Med* 2011;309:1205-10.
- [6] Linam LE, Darolia R, Naffaa LN, Breech LL, O'Hara S M, Hillard PJ, et al. US findings of adnexal torsion in children and adolescents: size really does matter. *Pediatr Radiol* 2007;3710:1013-9.
- [7] Servaes S, Zurakowski D, Laufer MR, Feins N, Chow JS. Sonographic findings of ovarian torsion in children. *Pediatr Radiol* 2007;375:446-51.
- [8] Jourjon R, Morel B, Irtan S, Audureau E, Coulomb-L'Hermine A, Larroquet M, et al. Analysis of clinical and ultrasound determinants of adnexal torsion in children and adolescents. *J*

Pediatr Adolesc Gynecol 2017;305:582-90.

[9] Beranger-Gibert S, Sakly H, Ballester M, Rockall A, Bornes M, Bazot M, et al. Diagnostic value of MR imaging in the diagnosis of adnexal torsion. Radiology 2016;2792:461-70.

[10] Ghossain MA, Hachem K, Buy JN, Hourany-Rizk RG, Aoun NJ, Haddad-Zebouni S, et al. Adnexal torsion: magnetic resonance findings in the viable adnexa with emphasis on stromal ovarian appearance. J Magn Reson Imaging 2004;203:451-62.

[11] Sadowski EA, Rockall AG, Maturen KE, Robbins JB, Thomassin-Naggara I. Adnexal lesions: imaging strategies for ultrasound and MR imaging. Diagn Interv Imaging 2019;10010:635-46.

[12] Landis JR, Koch GG. An application of hierarchical kappa-type statistics in the assessment of majority agreement among multiple observers. Biometrics 1977;332:363-74.

[13] Oltmann SC, Fischer A, Barber R, Huang R, Hicks B, Garcia N. Cannot exclude torsion: a 15-year review. J Pediatr Surg 2009;446:1212-6.

[14] Sintim-Damoa A, Majmudar AS, Cohen HL, Parvey LS. Pediatric ovarian torsion: spectrum of imaging findings. Radiographics 2017;376:1892-908.

[15] Rees MA, Squires JE, Tadros S, Squires JH. Canal of Nuck hernia: a multimodality imaging review. Pediatr Radiol 2017;478:893-8.

[16] Chiou SY, Lev-Toaff AS, Masuda E, Feld RI, Bergin D. Adnexal torsion: new clinical and imaging observations by sonography, computed tomography, and magnetic resonance imaging. J Ultrasound Med 2007;2610:1289-301.

- [17] Rialon KL, Wolf S, Routh JC, Adibe OO. Diagnostic evaluation of ovarian torsion: an analysis of pediatric patients using the Nationwide Emergency Department Sample. *Am J Surg* 2017;2134:637-9.
- [18] Hiller N, Appelbaum L, Simanovsky N, Lev-Sagi A, Aharoni D, Sella T. CT features of adnexal torsion. *AJR Am J Roentgenol* 2007;1891:124-9.
- [19] Swenson DW, Lourenco AP, Beaudoin FL, Grand DJ, Killelea AG, McGregor AJ. Ovarian torsion: case-control study comparing the sensitivity and specificity of ultrasonography and computed tomography for diagnosis in the emergency department. *Eur J Radiol* 2014;834:733-8.
- [20] Bader T, Ranner G, Haberlik A. Torsion of a normal adnexa in a premenarcheal girl: MRI findings. *Eur Radiol* 1996;65:704-6.
- [21] Cheng KL, Tsao TF. Ovarian torsion: appearance on MRI. *Pediatr Radiol* 2010;40 Suppl 1:S104.
- [22] Van Kerkhove F, Cannie M, Op de Beeck K, Timmerman D, Pienaar A, Smet MH, et al. Ovarian torsion in a premenarcheal girl: MRI findings. *Abdom Imaging* 2007;323:424-7.
- [23] Rha SE, Byun JY, Jung SE, Jung JI, Choi BG, Kim BS, et al. CT and MR imaging features of adnexal torsion. *Radiographics* 2002;222:283-94.
- [24] Valsky DV, Cohen SM, Hamani Y, Lipschuetz M, Yagel S, Esh-Broder E. Whirlpool sign in the diagnosis of adnexal torsion with atypical clinical presentation. *Ultrasound Obstet Gynecol* 2009;342:239-42.
- [25] Rousseau V, Massicot R, Darwish AA, Sauvat F, Emond S, Thibaud E, et al. Emergency management and conservative surgery of ovarian torsion in children: a report of 40 cases. *J*

Pediatr Adolesc Gynecol 2008;214:201-6.

[26] Santos XM, Cass DL, Dietrich JE. Outcome following detorsion of torsed adnexa in children. J Pediatr Adolesc Gynecol 2015;283:136-8.

[27] Kato H, Kanematsu M, Uchiyama M, Yano R, Furui T, Morishige K. Diffusion-weighted imaging of ovarian torsion: usefulness of apparent diffusion coefficient (ADC) values for the detection of hemorrhagic infarction. Magn Reson Med Sci 2014;131:39-44.

[28] Ozdemir O, Metin Y, Metin NO, Kupeli A. Contribution of diffusion-weighted imaging to conventional MRI for detection of haemorrhagic infarction in ovary torsion. BMC Med Imaging 2017;171:56.

[29] Rozenfeld MN, Podberesky DJ. Gadolinium-based contrast agents in children. Pediatr Radiol 2018;489:1188-96.

[30] Samanci C, Alis D, Ustabasioglu FE, Ozmen E, Ucar AK, Aslan M, et al. Apparent diffusion coefficient measurement of ovarian stroma: a potential tool for the diagnosis of polycystic ovary syndrome. Diagn Interv Imaging 2017;981:57-61.

## FIGURE/TABLE LEGENDS

**Figure 1:** Flow chart shows the patients inclusion/exclusion process into the study. AT = adnexal torsion; MRI = magnetic resonance imaging; US = ultrasound.

**Figure 2:** Adnexal torsion in a 13-year-old girl with a benign cystic mature teratoma. On ultrasonography (not shown), the right ovary could not be identified. **a**, T2-weighted MR image in sagittal plane shows an enlarged right ovary (black arrow), with parenchymal hyperintensity, peripheral distribution of follicles (arrowheads) and a whirlpool sign (white arrow). A mass with a cystic and solid component is identified. **b, c**, The presence of hyperintense fat signal (arrows) on axial T1-weighted sequences without (**b**) and with fat signal suppression (**c**) suggests ovarian teratoma. **d**, No enhancement of right ovary is observed after intravenous administration of a gadolinium chelate (d).

**Figure 3:** Left adnexal torsion in a 14-year-old menarcheal girl with a hemorrhagic cyst. **a**, Abdominal ultrasound image shows an enlarged left ovary (arrow) with a central hemorrhagic cyst (arrowheads). **b**, T2-weighted MR image in the axial plane confirms left ovary enlargement with a central cyst (arrow) and shows peripheral distribution of follicles (arrowheads) as well as global mild hyperintensity of the ovarian parenchyma and hyperintensity of the hemorrhagic cyst. **c**, T1-weighted MR image in the axial plane shows slightly hyperintense ovarian parenchyma (arrow). **d**, Subtracted T1-weighted MR image in the axial plane obtained after intravenous administration of a gadolinium chelate shows no enhancement of ovarian parenchyma (arrow). Surgery confirmed the left ovary ischemia

**Figure 4:** Hemorrhagic cyst in a 16-year-old girl. **a**, Abdominal ultrasound image shows enlarged ovary (arrows) with a central hemorrhagic cyst (arrowheads). The presence of an adnexal torsion on a hemorrhagic cyst could not be ruled out with ultrasound. **b, c**, MRI confirms the presence of hemorrhagic cyst (arrowheads on b and c). The parenchyma of the left ovary has a normal appearance on axial T2-weighted image (**b**) with a moderate stromal hyperintensity. On T1-weighted MR image in the sagittal plane (**c**), the ovarian parenchyma has a normal appearance and hemorrhagic cyst harbors fluid-fluid level (arrowheads). Moderate free peritoneal fluid is present (**b, c** and **d**). **d**, Fat suppressed T1-weighted MR image in the axial plane obtained intravenous administration of a gadolinium chelate shows normal enhancement of left ovary parenchyma (arrows) excluding ovarian torsion

**Figure 5:** Adnexal torsion with a paratubal cyst in a 13-year-old menarcheal girl. **a**, T2-weighted MR image in the sagittal plane shows a very large para-tubal cyst containing hemorrhage (arrowheads) and thickening of the right fallopian tube (arrow). **b**, T2-weighted MR image in the coronal plane shows enlarged right ovary with diffuse hypointensity of ovarian parenchyma (arrow). **c**, Diffusion-weighted MR image in the axial plane shows hyperintensity of right ovary (arrow) associated with hypointensity on ADC map (not shown). **D**, T1-weighted MR image in the axial plane obtained intravenous administration of a gadolinium chelate shows no enhancement of right ovary (arrow) suggesting ovarian ischemia.

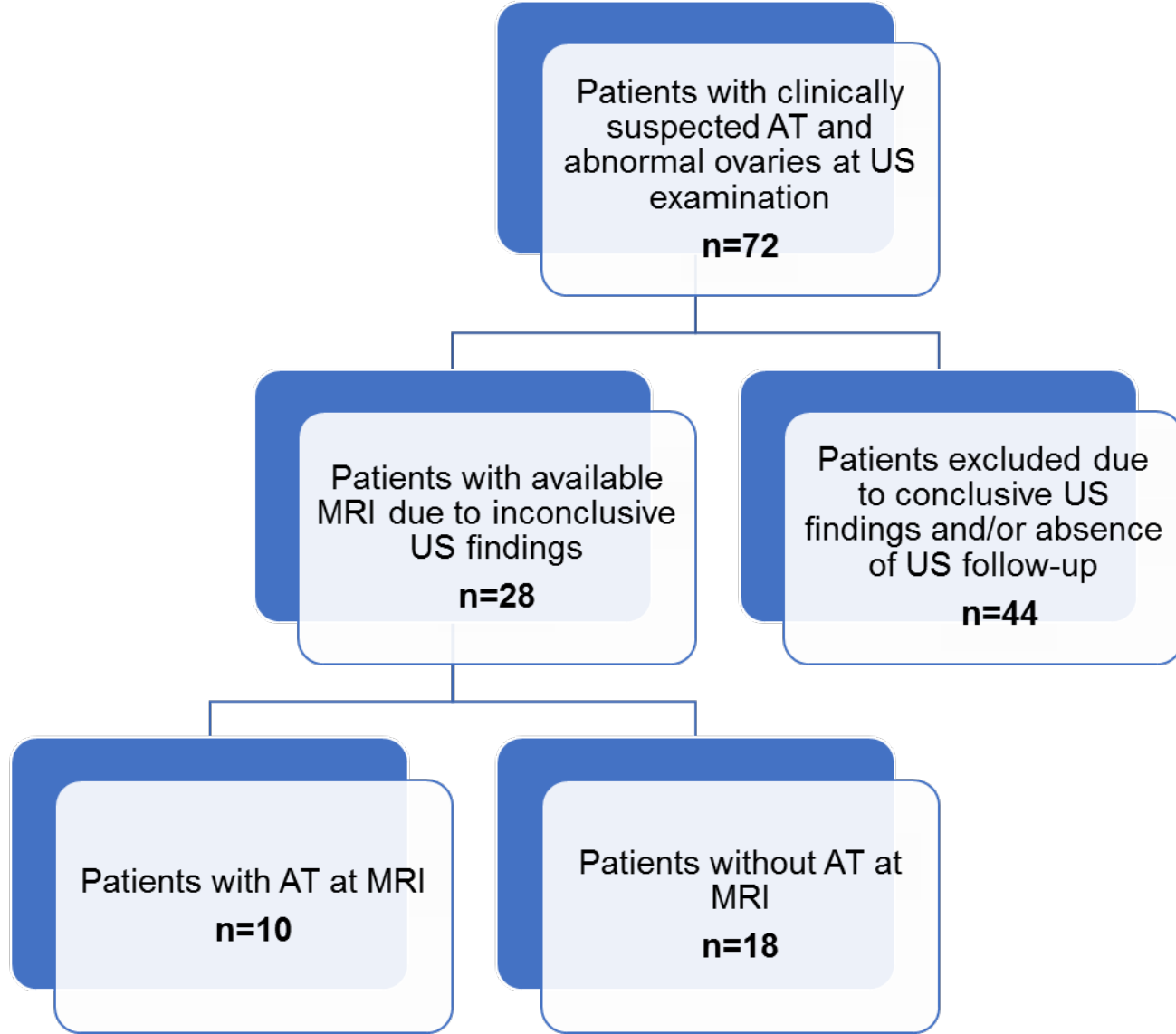
**Table 1.** Comparison of MRI findings for categorical variables between 18 children with no adnexal torsion and 10 children with adnexal torsion.

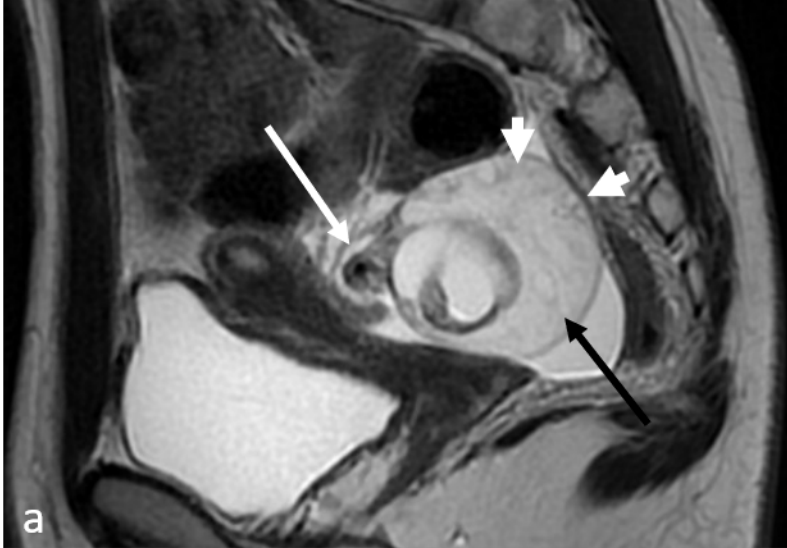
**Table 2.** Comparison of MRI findings for quantitative variables between 18 children with no adnexal torsion and 10 children with adnexal torsion.

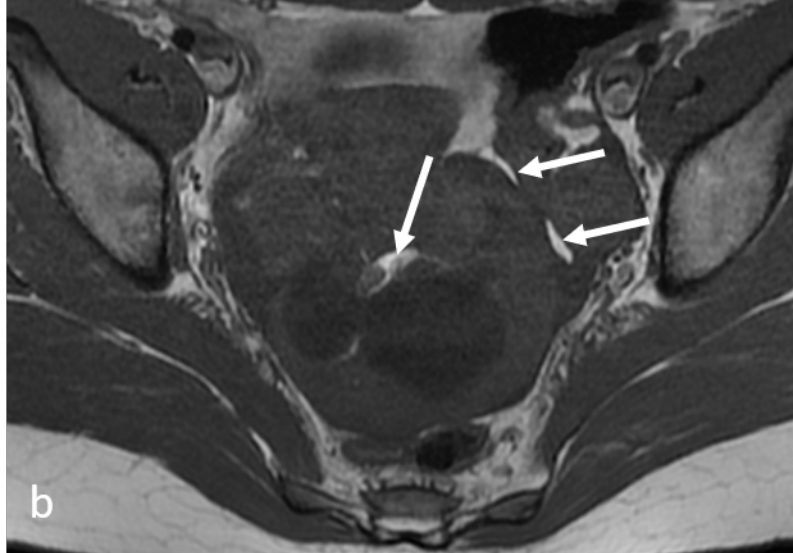
**Table 3.** Comparison of independent categorical criteria between patients with adnexal torsion and patients without adnexal torsion: results from exact logistic regression model.

**Table 4.** Sensitivity, specificity and accuracy of MRI criteria for the diagnosis of adnexal torsion.

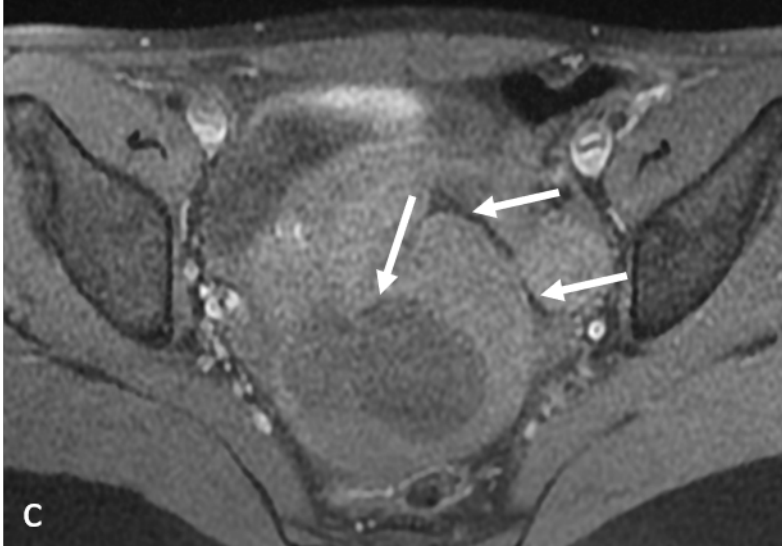
**Table 5.** Interobserver agreement for MRI features using an analytical method in the case of dichotomous variables.



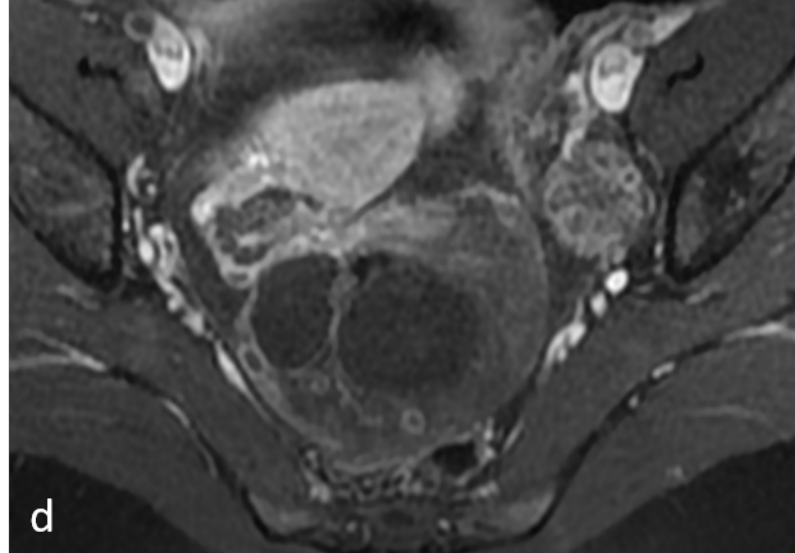




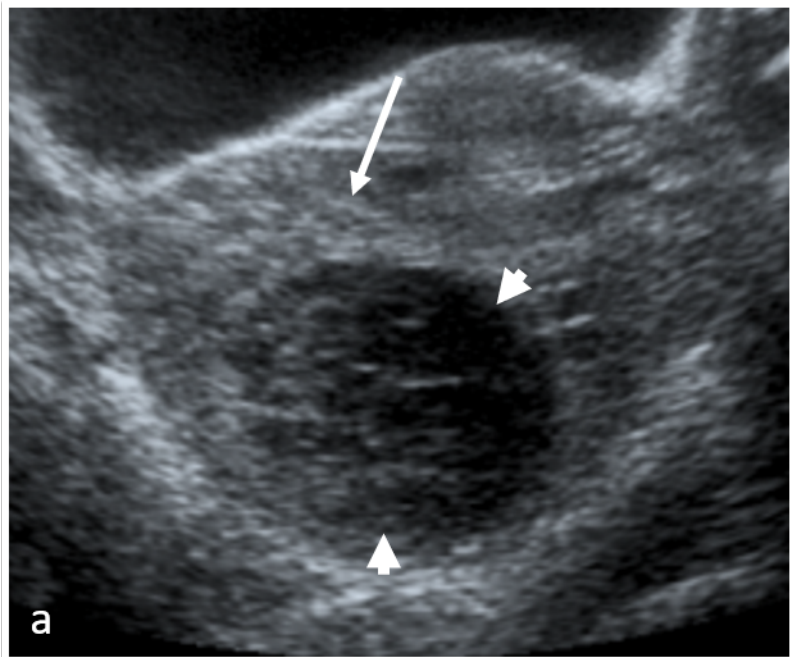
b

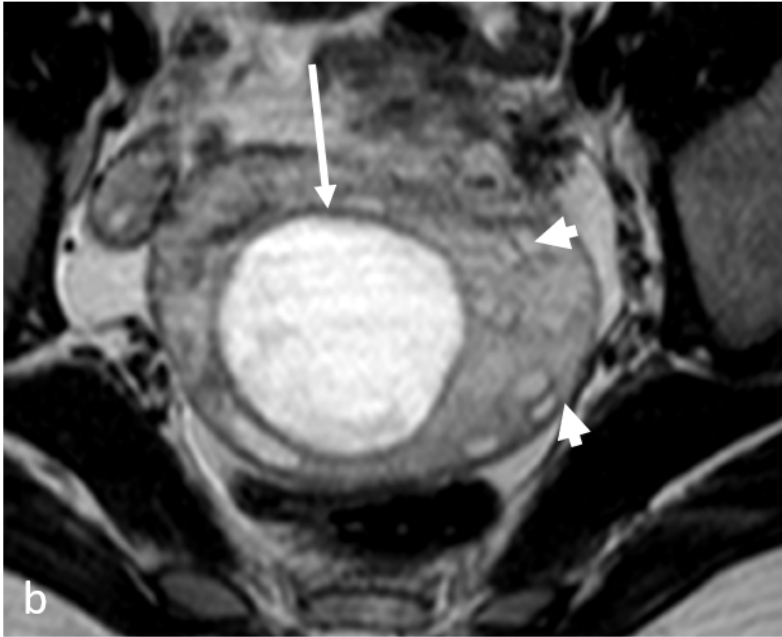


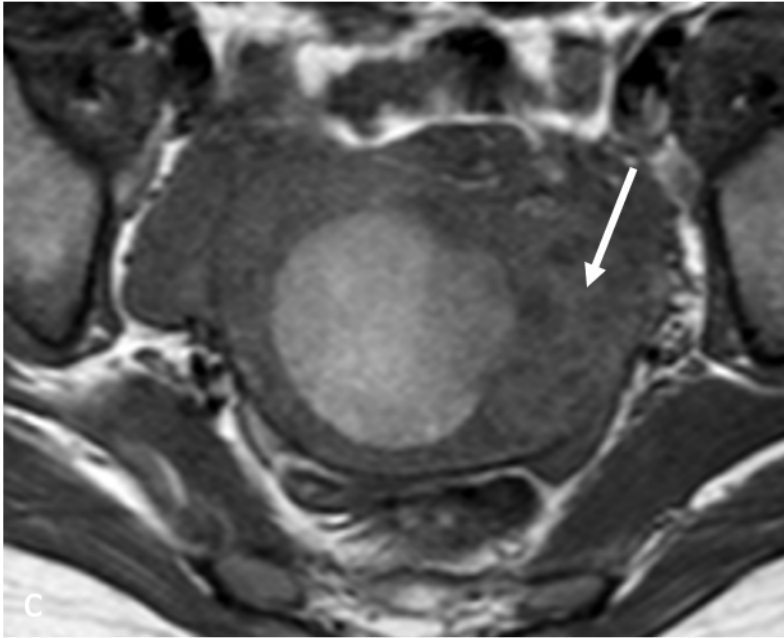
C



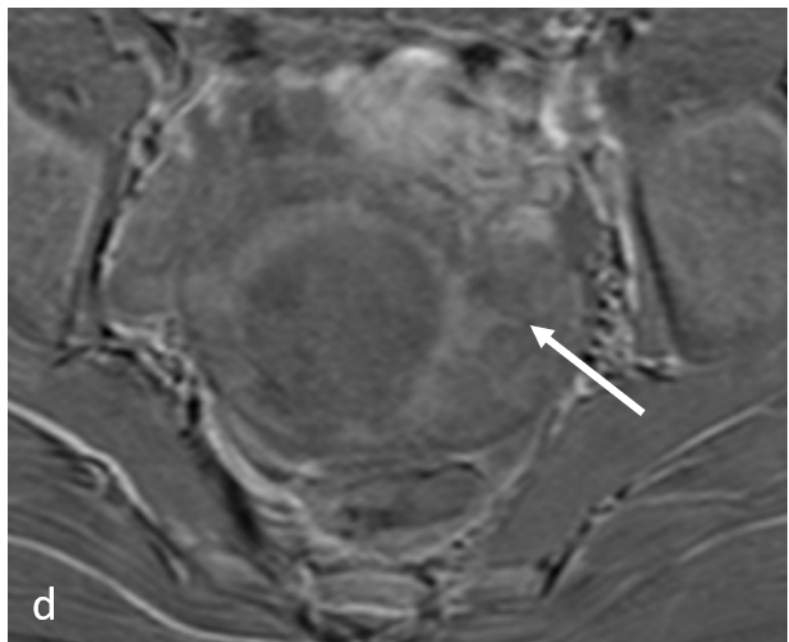
d

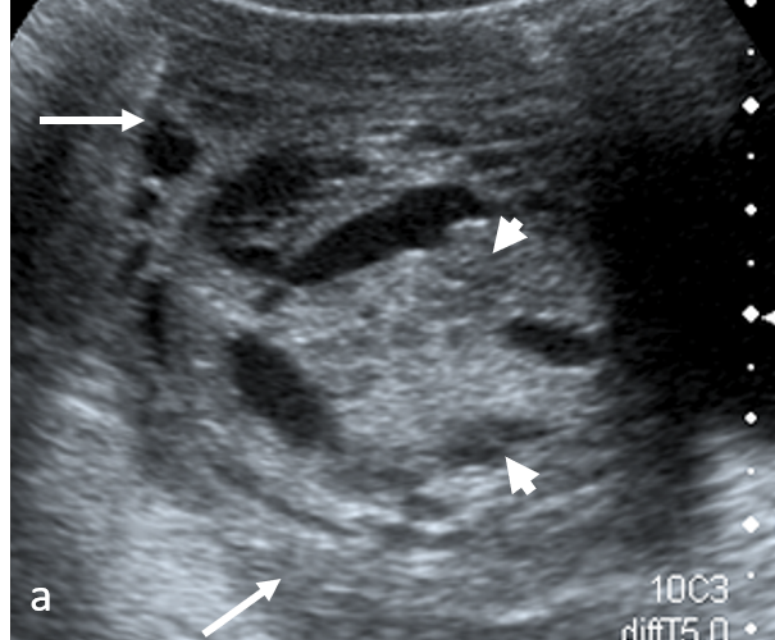






C



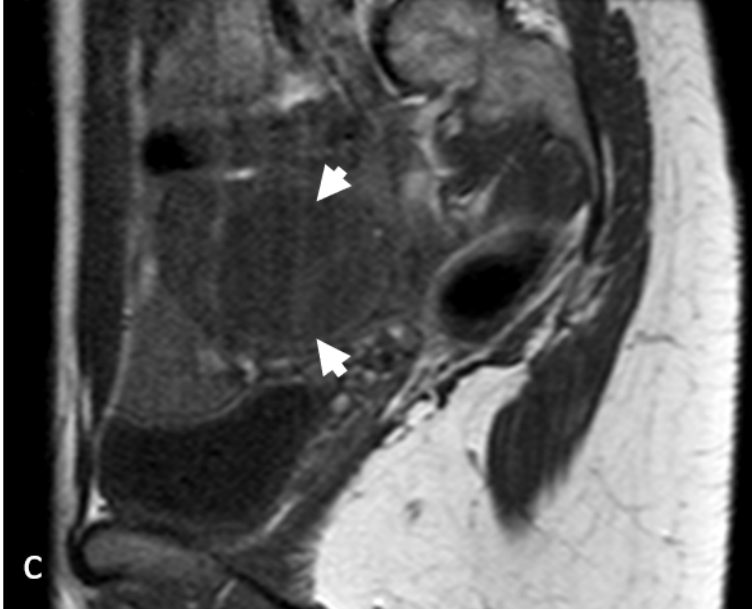


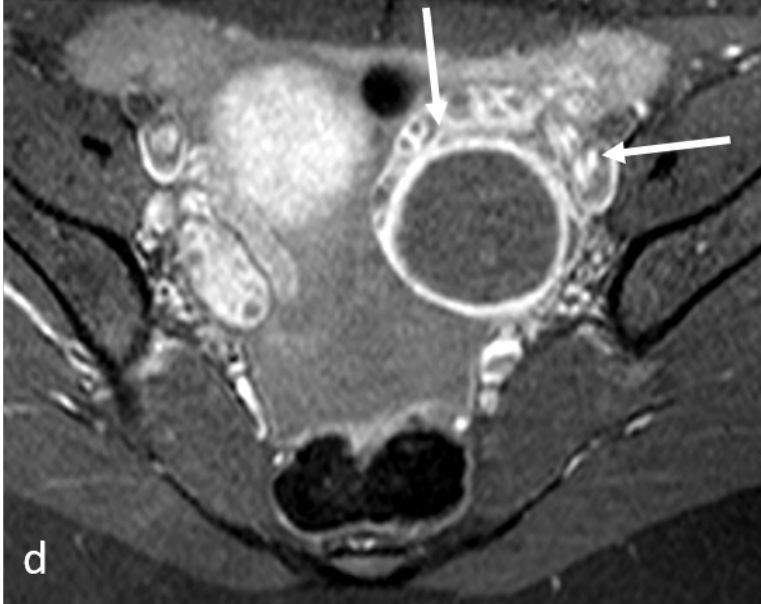
a

10C3

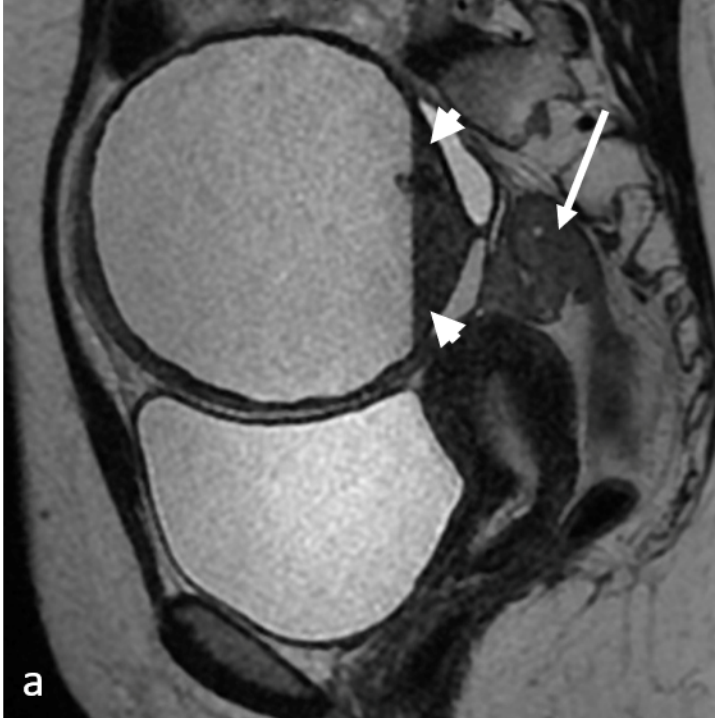
diffT5.0

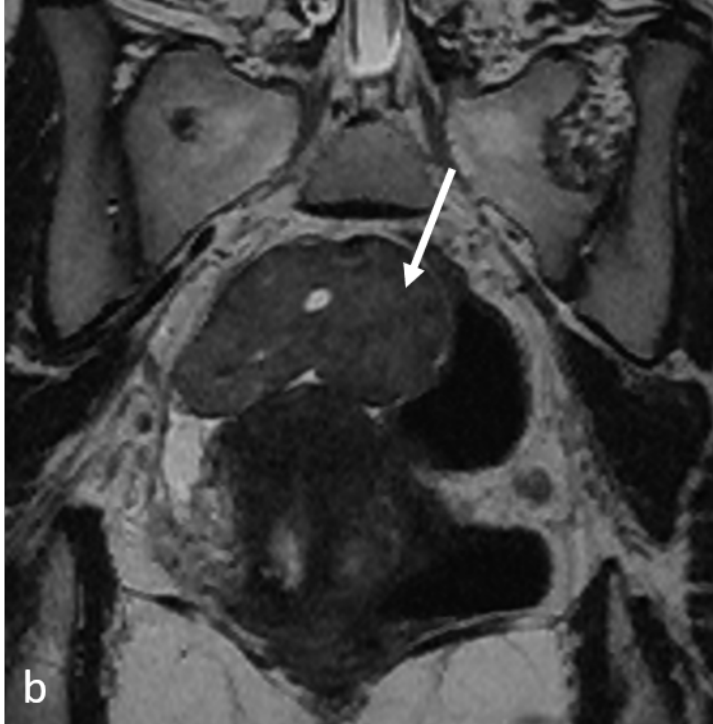


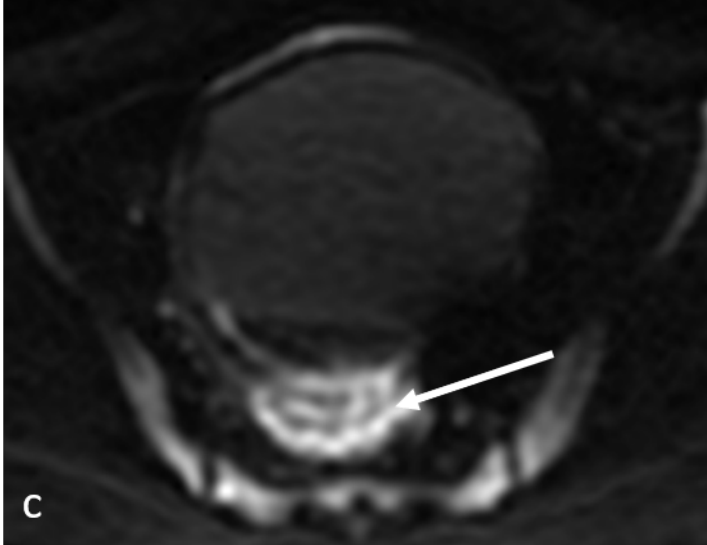


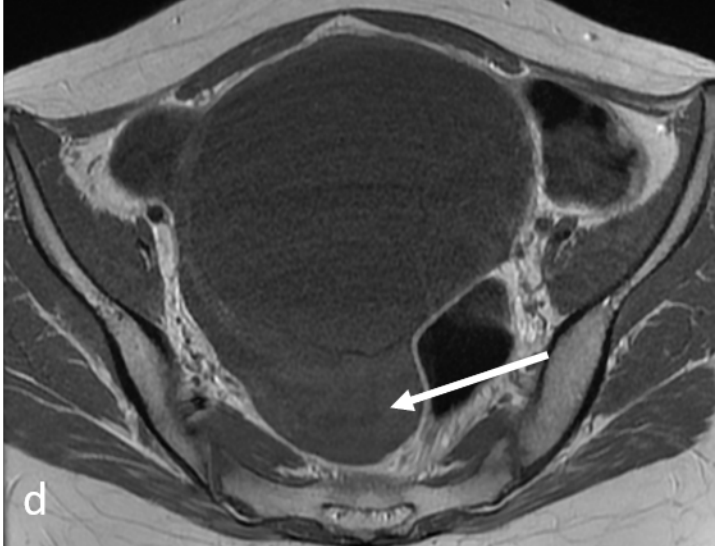


d









d

	No torsion	Torsion	P-value
<b>Ovary</b>			
<i>Ovarian T2 hyperintensity*</i>	10 (10/17; 59%)	5 (5/9; 56%)	> 0.999
<i>Ovarian T1 hyperintensity*</i>	0 (0/17; 0%)	3 (3/9; 33%)	<b>0.032</b>
<i>Peripheral distribution of follicles*</i>	14 (14/17; 82%)	7 (7/9; 78%)	> 0.999
<i>Asymmetric ovarian enhancement*</i>	2 (2/10; 20%)	6 (6/8; 75%)	0.054
<i>Ovarian shift to the involved side</i>	7 (7/18; 39%)	8 (8/10; 80%)	0.055
<b>Adnexa</b>			
<i>Tube thickening</i>	1 (1/18; 6%)	8 (8/10; 80%)	<b>&lt;0.001</b>
<i>Whirlpool sign</i>	0 (0/18; 0%)	8 (8/10; 80%)	<b>&lt;0.001</b>
<i>Tube dilatation</i>	1 (1/18; 6%)	2 (2/10; 20%)	0.284
<i>Asymmetric tubal enhancement*</i>	6 (6/12; 50%)	3 (3/9; 33%)	0.660
<i>Vascular pedicle enlargement</i>	1 (1/18; 6%)	4 (4/10; 40%)	<b>0.041</b>
<i>Uterine shift to the involved side</i>	3 (3/18; 17%)	4 (4/10; 40%)	0.207
<i>Pelvic fat infiltration*</i>	1 (1/12; 8%)	1 (1/8; 13%)	> 0.999
<b>Mass</b>			
<i>No mass</i>	2 (2/18; 11%)	4 (4/10; 40%)	0.147
<i>Multiple different tissues</i>	1 (1/18; 6%)	3 (3/10; 30%)	0.116
<i>Purely cystic</i>	0 (0/18; 0%)	1 (1/10; 10%)	> 0.999
<i>Cystic with hemorrhagic content</i>	15 (15/18; 83%)	2 (2/10; 20%)	<b>0.003</b>

Variables are expressed as raw numbers; numbers in parentheses are proportions followed by percentages. Bold indicates significance

\*For some variables, criteria were not assessable so that the denominator is different from 18 or 10.

	No torsion (n = 18)	Torsion (n = 10)	P-value
<b>Overall ovary (n=28)</b>			
<b>Axis length (cm)</b>			
Normal ovaries (n = 28)	3.22 ± 0.97 [2.00 - 5.70]	2.70 ± 0.97 [1.00 - 4.30]	0.280
Abnormal ovaries (n = 28)	5.03 ± 1.69 [2.80 - 10.5]	5.63 ± 2.80 [2.20 - 10.0]	0.962
Ratio (abnormal to normal)	0.68 ± 0.24 [0.32 - 1.34]	0.59 ± 0.29 [0.10 - 0.97]	0.632
<b>Surface area (cm<sup>2</sup>)</b>			
Normal ovaries (n = 28)	4.06 ± 2.64 [2.10 - 13.0]	3.42 ± 2.65 [0.40 - 8.90]	0.290
Abnormal ovaries (n = 28)	15.1 ± 12.1 [4.70 - 58.8]	20.1 ± 18.6 [2.46 - 53.0]	0.943
Ratio (abnormal to normal)	0.34 ± 0.24 [0.08 - 1.14]	0.37 ± 0.30 [0.01 - 0.88]	0.811
<b>Volume (cm<sup>3</sup>)</b>			
Normal ovaries (n = 28)	6.40 ± 7.94 [2.00 - 36.0]	4.22 ± 3.41 [0.25 - 10.6]	0.313
Abnormal ovaries (n = 28)	45.6 ± 59.9 [8.01 - 275.0]	84.4 ± 113.6 [2.40 - 320.0]	0.598
Ratio (abnormal to normal)	0.25 ± 0.31 [0.03 - 1.34]	0.31 ± 0.30 [0.01 - 0.88]	0.666
<b>If mass (n=22)</b>			
<b>Total ovary axis length (cm)</b>			
Normal ovaries (n = 22)	3.09 ± 0.94 [2.00 - 5.70]	2.98 ± 1.10 [1.00 - 4.30]	0.604
Abnormal ovaries (n = 22)	5.12 ± 1.75 [2.80 - 10.5]	7.35 ± 2.24 [3.50 - 10.0]	<b>0.042</b>
Ratio (abnormal to normal)	0.63 ± 0.19 [0.32 - 0.91]	0.48 ± 0.30 [0.10 - 0.97]	0.210
<b>Total ovary surface area (cm<sup>2</sup>)</b>			
Normal ovaries (n = 22)	3.74 ± 2.62 [2.10 - 13.0]	4.35 ± 3.12 [0.40 - 8.90]	0.505
Abnormal ovaries (n = 22)	15.6 ± 12.6 [4.70 - 58.8]	30.4 ± 17.5 [6.00 - 53.0]	<b>0.039</b>
Ratio (abnormal to normal)	0.29 ± 0.14 [0.08 - 0.59]	0.30 ± 0.34 [0.01 - 0.88]	0.507
<b>Total ovary volume (cm<sup>3</sup>)</b>			
Normal ovaries (n = 22)	5.82 ± 8.23 [2.00 - 36.0]	5.43 ± 4.03 [0.25 - 10.6]	0.606
Abnormal ovaries (n = 22)	47.5 ± 63.0 [8.01 - 275.0]	136.8 ± 122.5 [8.20 - 320.0]	0.121
Ratio (abnormal to normal)	0.19 ± 0.16 [0.03 - 0.61]	0.20 ± 0.29 [0.01 - 0.74]	0.338
<b>Mass dimensions</b>			
Axis length (cm) (n = 22)	4.01 ± 2.12 [1.40 - 10.5]	8.18 ± 2.77 [4.30 - 11.3]	<b>0.004</b>
Surface area (cm <sup>2</sup> ) (n = 22)	11.5 ± 13.5 [1.50 - 58.8]	44.0 ± 28.2 [12.5 - 86.0]	<b>0.004</b>
Volume (cm <sup>3</sup> ) (n = 22)	33.3 ± 65.4 [1.20 - 275.0]	241.5 ± 196.9 [24.0 - 547.0]	<b>0.003</b>

<b><i>Ovary-corrected surface area (cm<sup>2</sup>)</i></b>			
Abnormal surface area (n = 20)	4.12 ± 1.85 [0.01 - 7.10]	9.88 ± 9.73 [2.00 - 22.0]	0.705
Ratio (abnormal to normal) (n=20)	0.95 ± 0.96 [0.42 - 4.33]	0.51 ± 0.52 [0.11 - 1.25]	0.109
<b><i>Ovary-corrected volume (cm<sup>3</sup>)</i></b>			
Abnormal volume (n = 20)	14.2 ± 9.0 [0.01 - 38.0]	51.0 ± 34.0 [10.0 - 91.0]	<b>0.047</b>
Ratio (abnormal to normal) (n = 20)	0.35 ± 0.24 [0.13 - 0.95]	0.11 ± 0.10 [0.01 - 0.22]	<b>0.021</b>

Bold indicates significant P value

Variables are expressed as means ± standard deviations; numbers in brackets are ranges

Parameter		No torsion	Torsion	Odds ratio (95% CI)	P-value	AUC
<b>Global</b>	Diagnosis of torsion with MRI	1/18 (6%)	10/10 (100%)	<b>106.1</b> (12.0)	<b>&lt; 0.0001</b>	0.97
	Age (years) <13	2/18 (11%)	6/10 (60%)	<b>10.7</b> (1.3; 148.2)	<b>0.022</b>	0.74
<b>Ovary</b>	Ovarian T1 hyperintensity	0/17 (0%)	3/9 (33%)	9.0 (0.9) *	0.065	0.67
	Asymmetrical ovarian enhancement	2/10 (20%)	6/8 (75%)	10.0 (0.9; 188.4)	0.061	0.77
	Ovarian shift to the involved side	7/18 (39%)	8/10 (80%)	5.9 (0.8; 72.7)	0.087	0.71
<b>Adnexa</b>	Tube thickening	1/18 (6%)	8/10 (80%)	<b>51.0</b> (4.2; 3181.6)	<b>&lt; 0.0001</b>	0.87
	Whirlpool sign	0/18 (0%)	8/10 (80%)	<b>61.0</b> (7.2) *	<b>&lt; 0.0001</b>	0.90
	Vascular pedicle enlargement	1/18 (6%)	4/10 (40%)	10.2 (0.8; 589.8)	0.082	0.67
<b>Mass</b>	Absence of cystic mass with hemorrhagic content	3/18 (17%)	8/10 (80%)	<b>17.1</b> (2.1; 248.4)	<b>0.004</b>	0.82
	Mass volume ( $\geq 30$ cm <sup>3</sup> )	2/16 (13%)	5/6 (83%)	<b>26.7</b> (1.9; 1766.6)	<b>0.009</b>	0.85
	Mass surface area ( $\geq 14$ cm <sup>2</sup> )	2/16 (13%)	4/6 (67%)	11.7 (1.0; 224.9)	0.051	0.77
	Mass axis length ( $\geq 5$ cm)	3/16 (19%)	5/6 (83%)	<b>17.9</b> (1.4; 1100.1)	<b>0.022</b>	0.82
	Abnormal ovary-corrected volume ( $\geq 30$ cm <sup>3</sup> )	1/16 (6%)	3/4 (75%)	<b>29.6</b> (1.3; 2507.2)	<b>0.027</b>	0.84
	Ovary-corrected volume ratio (<0.2)	4/15 (27%)	3/4 (75%)	7.2 (0.4; 471.3)	0.235	0.74

AUC: area under the receiver operating characteristics curve. **Bold** odds ratios are statistically significant at  $P < 0.05$

Unadjusted odds ratios (95% confidence interval) from exact logistic regression modeling.

\*For cells with null percentages (i.e. ovarian T1 hyperintensity, whirlpool sign), median unbiased estimates are provided.

Parameter	TP	TN	FP	FN	Sensitivity	Specificity	Accuracy	
<b>Global</b>	Diagnosis of torsion with MRI	10	17	1	0	100% (10/10) [69 - 100]	94% (17/18) [73 - 100]	96% (27/28) [82 - 100]
	Age <13 years*	6	16	2	4	60% (6/10) [26 - 88]	89% (16/18) [65 - 99]	79% (22/28) [59 - 92]
<b>Ovary</b>	Ovarian T1 hyperintensity	3	17	0	6	33% (3/9) [7 - 70]	100% (17/17) [80 - 100]	77% (20/26) [56 - 91]
	Asymmetrical ovarian enhancement	6	8	2	2	75% (6/8) [35 - 97]	80% (8/10) [44 - 97]	78% (14/18) [52 - 94]
	Ovarian shift to the involved side	8	11	7	2	80% (8/10) [44 - 97]	61% (11/18) [36 - 83]	68% (19/28) [48 - 84]
<b>Adnexa</b>	Tube thickening	8	17	1	2	80% (8/10) [44 - 97]	94% (17/18) [73 - 100]	89% (25/28) [72 - 98]
	Whirlpool sign	8	18	0	2	80% (8/10) [44 - 97]	100% (18/18) [81 - 100]	93% (26/28) [76 - 99]
	Vascular pedicle enlargement	4	17	1	6	40% (4/10) [12 - 74]	94% (17/18) [73 - 100]	75% (21/28) [55 - 89]
<b>Mass</b>	Absence of cystic mass with hemorrhagic content	8	15	3	2	80% (8/10) [44 - 97]	83% (15/18) [59 - 96]	82% (23/28) [63 - 94]
	Mass volume ( $\geq 30 \text{ cm}^3$ )*	5	14	2	1	83% (5/6) [36 - 100]	88% (14/16) [62 - 98]	86% (19/22) [65 - 97]
	Mass surface area ( $\geq 14 \text{ cm}^2$ )*	4	14	2	2	67% (4/6) [22 - 96]	88% (14/16) [62 - 98]	82% (18/22) [60 - 95]
	Mass axis length ( $\geq 5 \text{ cm}$ )*	5	13	3	1	83% (5/6) [36 - 100]	81% (13/16) [54 - 96]	82% (18/22) [60 - 95]
	Abnormal ovary-corrected volume ( $\geq 30 \text{ cm}^3$ )*	3	15	1	1	75% (3/4) [19 - 99]	94% (15/16) [70 - 100]	90% (18/20) [68 - 99]
	Ovary-corrected volume ratio ( $< 0.2$ )*	3	11	4	1	75% (3/4) [19 - 99]	73% (11/15) [45 - 92]	74% (14/19) [49 - 91]

TP = true positive; TN = true negative, FP = false positive, FN = false negative

\* Quantitative variables were dichotomized after optimal thresholds were determined by identifying the value with the maximal Youden's index and the shortest distance from the upper-left corner on ROC analysis. Sensitivity, specificity and accuracy are expressed as percentages; numbers in parentheses are proportions; followed by 95% confidence intervals into brackets.

<b>Parameter</b>	<b>Agreement</b>	<b>Kappa (95% CI)</b>	<b>Corresponding rating</b>	
<b>Global</b>	Diagnosis of torsion with MRI	100% (28/28)	1.00 (1.00; 1.00)	Perfect
<b>Ovary</b>	Ovarian T2 hyperintensity	73% (19/26)	0.48 (0.17; 0.79)	Moderate
	Ovarian T1 hyperintensity	92% (24/26)	0.47 (-0.13; 1.00)	Moderate
	Peripheral distribution of follicles	77% (20/26)	0.36 (-0.05; 0.76)	Fair
	Asymmetrical ovarian enhancement (n=18)	78% (14/18)	0.55 (0.16; 0.94)	Moderate
	Ovarian shift to the involved side	75% (21/28)	0.48 (0.19; 0.76)	Moderate
<b>Adnexa</b>	Tube thickening	93% (26/28)	0.83 (0.60; 1.00)	Almost perfect
	Whirlpool sign	86% (24/28)	0.62 (0.29; 0.95)	Substantial
	Vascular pedicle enlargement	82% (23/28)	0.00 (0.00; 0.00)	Slight
<b>Mass</b>	Absence of cystic mass with hemorrhagic content	93% (25/27)	0.85 (0.65; 1.00)	Almost perfect
	Mass volume ( $\geq 30\text{cm}^3$ ) (n = 22)	86% (19/22)	0.72 (0.43; 1.00)	Substantial
	Mass surface ( $\geq 14\text{cm}^2$ ) (n = 22)	82% (18/22)	0.58 (0.23; 0.94)	Moderate
	Mass axis ( $\geq 5\text{cm}$ ) (n = 22)	95% (21/22)	0.90 (0.71; 1.00)	Almost perfect
	Abnormal ovary corrected volume ( $\geq 30\text{ cm}^3$ )	89% (17/19)	0.6 (0.14; 1.00)	Substantial
	Ovary-corrected volume ratio (< 0.2)	83% (15/18)	0.62 (0.26; 0.98)	Substantial